1 Introduction

The goal of this work is to optimize the design and control of a soft, passive tentacle swimmer to maximize average thrust and velocity. Modeling and understanding the fluid-structure interactions between compliant soft bodies and water is highly complex, resulting in nonlinear behavior that makes these systems difficult to describe analytically. A data-driven approach is therefore required, leveraging a large number of simulations to train surrogate models and optimize the objectives. The simulated data, although not experimentally validated, are expected to capture the correct trends and orders of magnitude, making them suitable for guiding preliminary design decisions. Based on this, the study aims to support the future development of energy-efficient, compliant swimmers for underwater exploration or inspection tasks.

2 Design problem

The passive tentacle is actuated in one degree of freedom, following a pitching motion around the axis normal to the base. As shown in Figure 1, the tentacle geometry is characterized by its length l (between 0.1 and 1 m), fixed decreasing diameters ($d_{\text{base}} = 0.02$ m, $d_{\text{tip}} = 0.005$ m), and a composition ratio c (between 0 and 1), which defines the relative length of two materials with different stiffnesses: Dragon Skin™ (stiffer) and Ecoflex™. The control input is a sawtooth signal with amplitude A (between 5° and 135°) and frequency f (between 0.05 and 10 Hz), defined through its truncated Fourier series as:

$$A(t) = A - A \cdot \left(\frac{1}{2} - \frac{1}{\pi} \sum_{k=0}^{3} \frac{(-1)^k \sin\left(2\pi(k+1)ft\right)}{k+1} \right)$$

This asymmetric signal is designed to generate a non-zero average thrust: the tentacle extends slowly and recoils rapidly, resulting in a stronger fluid reaction during the retraction phase.

The design is optimized with respect to two key performance objectives: average thrust and forward velocity. These objectives are partially correlated but not equivalent, and optimizing both enables the identification of trade-offs between force generation and movement speed. It is worth noting that the product of thrust and velocity corresponds to the mechanical propulsion power delivered to the fluid.

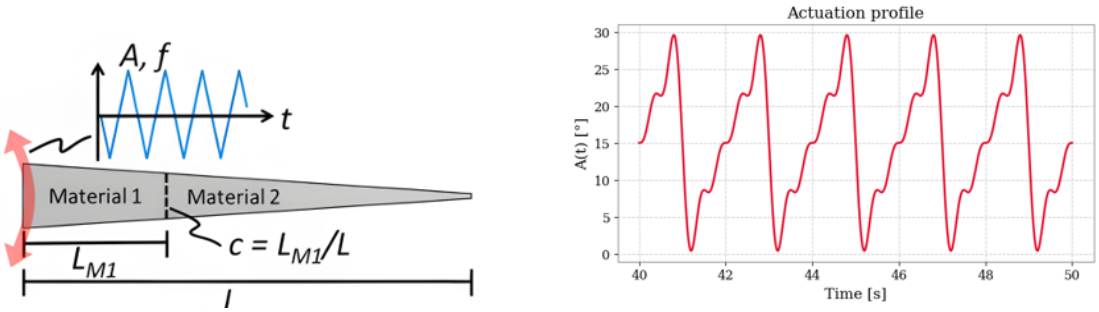

Figure 1: Encoding variables and actuation profile

Since the size of the design space is relatively small (four parameters: l, c, A, and f), and no evident correlation exists between the parameters to be optimized, dimensionality reduction is neither performed nor required.

Given the relatively short runtime of each simulation (less than 20 seconds), the initial dataset used to train the surrogate model was generated through a full factorial Design of Experiments, using uniform discretization over the four key parameters. Each parameter was sampled uniformly, and all combinations were simulated, resulting in a dense parameter grid (grid size of 8 per dimension).

3 Data capture

Data were obtained from simulations over one minute of tentacle motion, and the average thrust and velocity were computed. Figure 2 shows the multibody modeling and actuation of the soft structure, together with the simulated behavior for $l = 0.5$ m, $c = 0.5$, $f = 3$ Hz, and $A = 45°$. The periodic nature of the actuation is clearly visible, along with the initial transient caused by inertial effects, which motivates the use of long simulation times to obtain reliable average values.

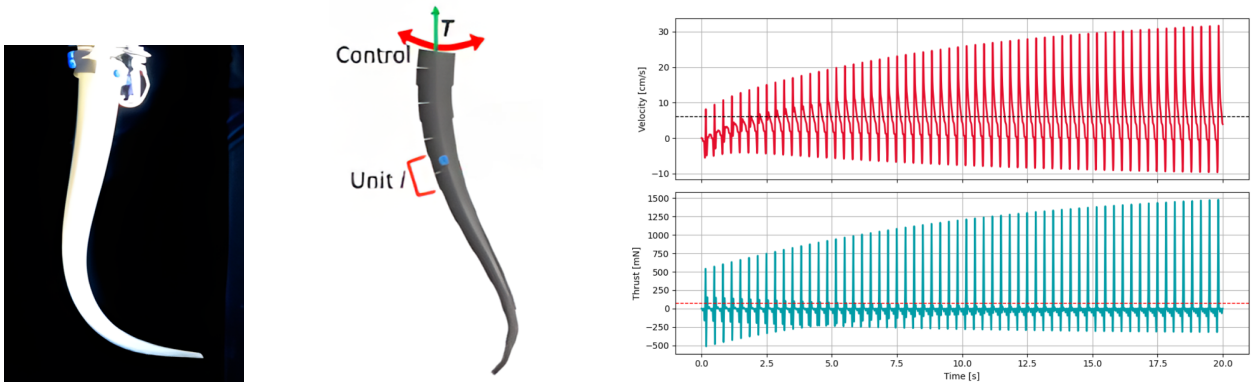

Figure 2: Soft tentacle, multibody simulation and results

Using a lumped-parameter method [1], the tentacle is discretized into a set of frustum-shaped masses, connected to each other by torsional springs and dampers, which allow for bending deformation of the soft body. Each mass has a length of 2.5 cm. The silicone parameters (listed in Table 1) are estimated from commercial data, the drag coefficient is taken from [1], and both the spring coefficient and the moment of inertia are derived from standard beam theory (see Table 2).

Table 1: Material and fluid parameters

Parameter	Value
Silicone density (kg/m^3)	1070
Ecoflex™ E (Pa)	$8.0 \cdot 10^3$
Dragon Skin™ E (Pa)	$4.25 \cdot 10^4$
Ecoflex™ damping factor (N·m·s/rad)	0.05
Dragon Skin™ damping factor (N·m·s/rad)	0.10
C_D	2.0

Table 2: Beam-theory-based quantities

Quantity	Expression
Mass moment of inertia	$I_i = \frac{1}{12} m_i L_i^2$
Geometric moment of inertia	$J_i = \frac{\pi \bar{d}_i^4}{64}$
Spring coefficient	$k_i = \frac{3 E_i J_i}{4 L_i}$

For each element, hydrodynamic, elastic, and damping moments contribute to inertia as follows:

$$\alpha_i = -\frac{M^{\text{stiff}}_{\text{left},i} + M^{\text{stiff}}_{\text{right},i} + M^{\text{damp}}_{\text{left},i} + M^{\text{damp}}_{\text{right},i} + M^{\text{hydro}}_i}{I_i}$$

$$M^{\text{stiff}}_{\text{left},i} = k_i(\theta_i - \theta_{i-1}), \quad M^{\text{stiff}}_{\text{right},i} = k_{i+1}(\theta_{i+1} - \theta_i)$$

$$M^{\text{damp}}_{\text{left},i} = b_i(\omega_i - \omega_{i-1}), \quad M^{\text{damp}}_{\text{right},i} = b_{i+1}(\omega_{i+1} - \omega_i)$$

$$M^{\text{hydro}}_i = \frac{1}{12}\rho_w C_D A_{\text{lat},i} L_i^2 \frac{U^{\perp}_{i+1} - U^{\perp}_i}{L_i} \frac{U^{\perp}_{i+1} + U^{\perp}_i}{2}$$

For each time step, thrust and velocity are then computed as:

$$\begin{cases} T(t) = F_{\text{drag}}(t) + F_{\text{added mass}}(t) \\ v(t) = \displaystyle\int_0^t \frac{T(\tau) - F_{\text{resist}}(v(\tau))}{m}\, d\tau \end{cases}$$

A stiff implicit integrator (BDF method from `solve_ivp`) is used with high temporal resolution (60,000 points) and strict tolerances (`atol` $= 10^{-6}$, `rtol` $= 10^{-4}$).

The simulation data is noise-free and fully deterministic; while this ensures consistency across runs, it does not account for real-world variability. The use of high temporal resolution (60,000 steps per minute) ensures accuracy but comes at the cost of increased simulation time. As anticipated in Section 1, these results have not been experimentally validated; although they reflect realistic behavior, they should be interpreted as idealized predictions of the system's performance.

4 Data-driven method

The adopted data-driven optimization pipeline is shown in Figure 3. Initial data are collected through full factorial DoE and used to train an artificial neural network surrogate model. The architecture is a multi-layer perceptron with two hidden layers, which regresses thrust and velocity as functions of the design space parameters. It is trained using `MSE` loss, `Adam` optimizer with learning rate $\eta = 10^{-3}$, and early stopping with a 90-10% split.

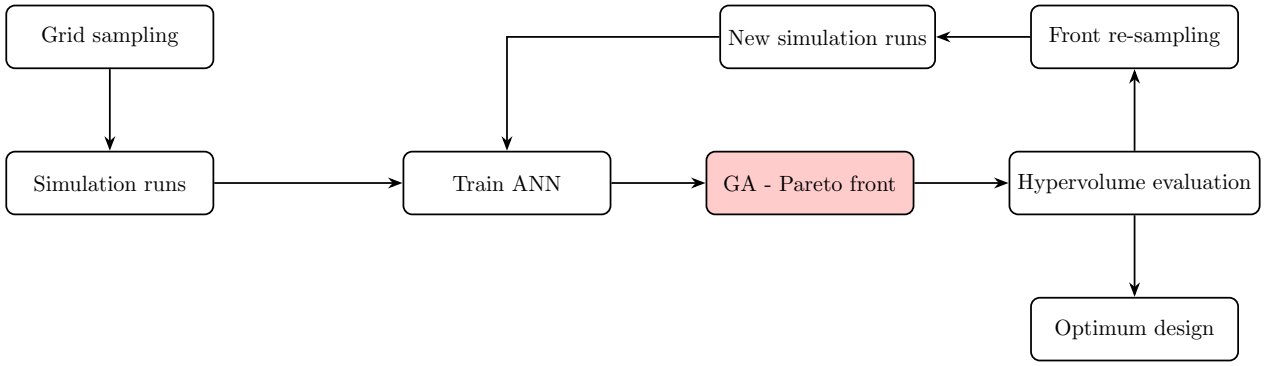

Figure 3: Data-driven optimization

A multi-objective Genetic Algorithm is chosen to optimize two conflicting objectives in a framework where direct access to an analytical formulation of the objective function is not available, and the design space is explored through a population of individuals. The population size is set to 100 to ensure sufficient coverage of the design space without incurring excessive computational cost; the crossover probability is set to 0.9 to maintain high evolutionary pressure toward new configurations and to approximate the Pareto front effectively from the first generations; the mutation rate is set to 1/4 so that, on average, one variable is mutated per individual per generation. This method minimizes the vector `[-thrust, -velocity]` to obtain the Pareto front.

Once the optimization for a given dataset is completed, *active learning* is implemented: Pareto points are perturbed with Gaussian noise, and simulations are performed for all of them to enrich the dataset with informative samples, in order to better exploit the most promising regions of the design space. Once the new dataset is collected (adding 50 new samples at each iteration), the surrogate model is retrained and the optimization is repeated. Variable perturbations are assumed to be independent, with standard deviations for l, c, f, and A equal to 0.2 m, 0.2, 0.4, and 10°, respectively.

The stopping criterion is based on hypervolume evaluation. Hypervolumes measure the portion of the objective space (`[-thrust, -velocity]`) dominated by the Pareto front with respect to a fixed reference

point, here set to `[0, 0]`. Active learning stops when this metric reaches a *plateau*, that is, when the optimization process no longer yields a diverse distribution. In practice, this occurs when Δ_{HV} (the absolute difference between successive hypervolumes) remains below 0.05 for 5 consecutive iterations.

Figure 4 shows the training and validation losses, the Pareto front at the final iteration (79^{th}), and the evolution of Δ_{HV} across iterations, which naturally decreases in a non-monotonic way due to the stochastic nature of the process.

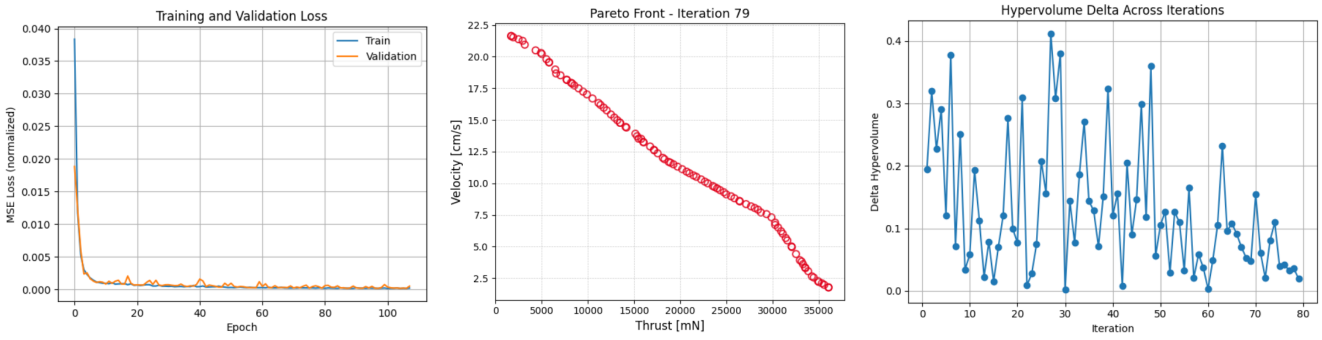

Figure 4: Surrogate model training, final Pareto front, and Δ_{HV} over iterations

5 Results

Table 3: Best results by objective

Objective	c	A [°]	f [Hz]	l [m]
Thrust	0.818	135.0	10.0	1.0
Velocity	0.752	49.7	10.0	0.95
Power	0.000	116.5	10.0	1.0

Table 4: Pareto front summary statistics

Metric	Min	Max	Mean
Thrust [N]	1.86	34.82	19.12
Velocity [cm/s]	1.83	21.66	12.05
Power [W]	0.40	2.25	1.72

Results from the multi-objective Genetic Algorithm optimization are shown in Table 3. As expected, maximum thrust, velocity, and power are achieved for $f = 10$ Hz and l very close to 1 m, since propulsion is generated at a higher average peripheral speed (although the optimal velocity occurs at $l = 0.95$ m, suggesting that saturation has been reached due to the robot's passivity). Meanwhile, the high frequency contributes by generating more thrust cycles per unit time. Note that the motor is assumed ideal, capable of reproducing all motions without limitations; additional constraints would have affected the result.

More interestingly, the composition ratio c leads to higher thrust and velocity at high values, resulting in stiffer structures. However, maximum velocity is achieved with a lower amount of Dragon Skin$^{\text{TM}}$, suggesting that more compliant structures likely offer less resistance to the fluid. Maximum power, on the other hand, is achieved with all Ecoflex$^{\text{TM}}$, where the tentacle moves more freely and thus transfers more mechanical energy to the surrounding fluid. Conversely, the amplitude $A°$ is maximized for highest thrust (benefiting from the steeper regions of the sawtooth), while it is kept low for velocity to reduce resistance, and set to intermediate values for power.

Table 4 shows the value ranges of the Pareto front, representing the best compromise results. Notably, thrust and velocity exhibit wide ranges, as optimizing one can lead to suboptimal values of the other. This is consistent, as one might expect, with swimming techniques: swimmers must not only generate significant propulsion, but also adapt their body and motion to the fluid to minimize resistance and increase their speed.

Obayashi et al. [1] report an optimal velocity of 6.2 cm/s for a different tentacle robot with a distinct actuation configuration. Although the setup differs, most notably in tentacle length (1 m vs 20 cm) and motion profile, the reported velocity is of the same order of magnitude as those shown in the table. This

suggests that the *sim2real* gap may not be insurmountable. Also note that the increase in speed is not linear, as the system is passive and bends in response to fluid interaction (see Figure 8 for further details).

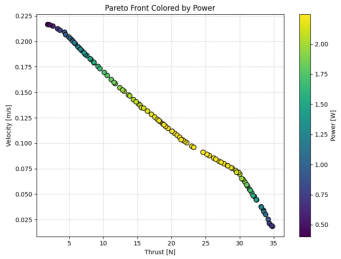

Figure 5: Pareto front colored by generated power

Figure 5 shows the Pareto front in relation to the generated power, which is naturally higher where the product of the two objective functions is greater. Figure 6 illustrates the effects of all parameters on thrust and velocity across the Pareto front. While lower values of c dominate the front (corresponding to higher power), the highest individual objectives are achieved at higher material ratios. Thrust increases with amplitude, whereas velocity starts from its maximum and decreases as amplitude increases. Optimal frequencies and lengths are consistently concentrated at their highest values.

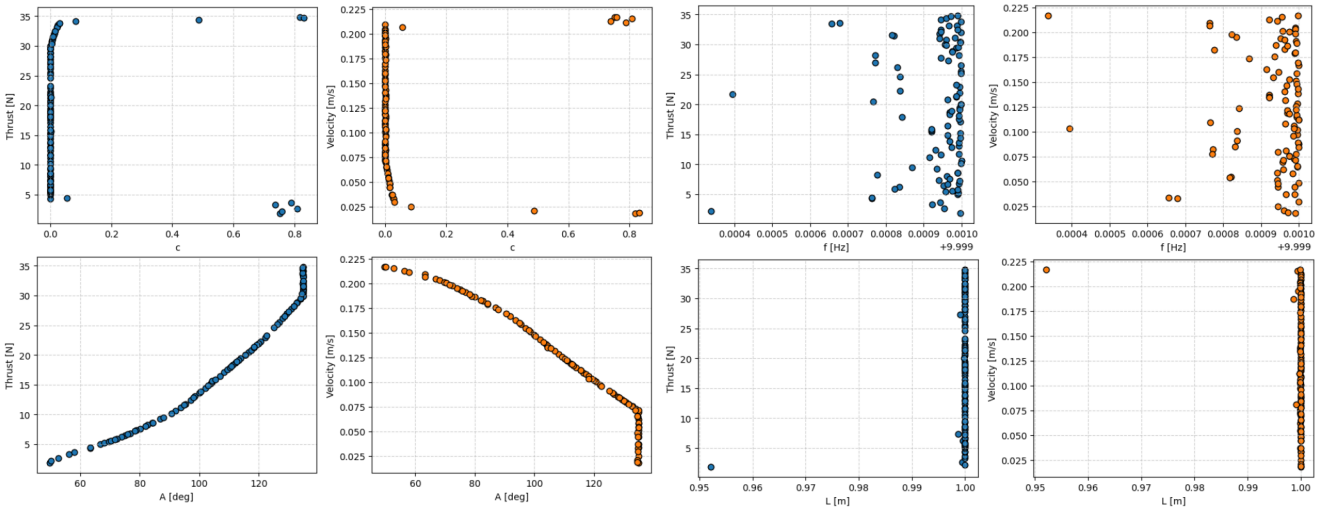

Figure 6: Effects of design parameters on thrust and velocity (Pareto front)

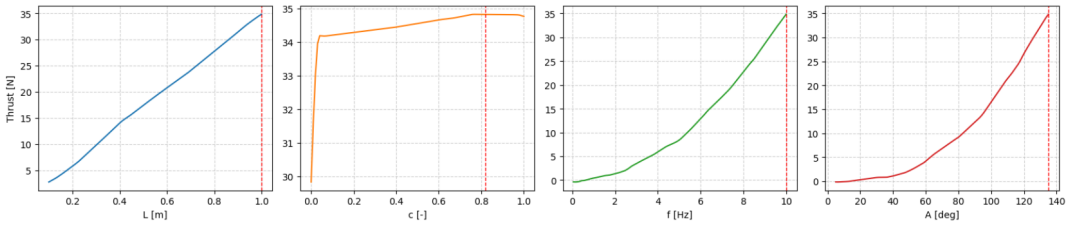

Figure 7: Optimal thrust vs. L, c, f, A

Figures 7, 8, and 9 each fix three parameters to their respective optimal values for thrust, velocity, and power, and use the surrogate model to analyze how the target quantity varies with respect to the remaining parameter. Regarding l, it is interesting to observe that velocity reaches a *plateau* after its maximum, indicating that longer tentacles can no longer accelerate the robot, as the structure's compliance causes

the tip to lag behind. Increasing the material ratio c clearly reduces power and produces a distinct peak in velocity, while its effect on thrust is less pronounced. Frequency consistently displays a monotonic trend, while amplitude has a positive effect on thrust and shows a distinct peak for velocity.

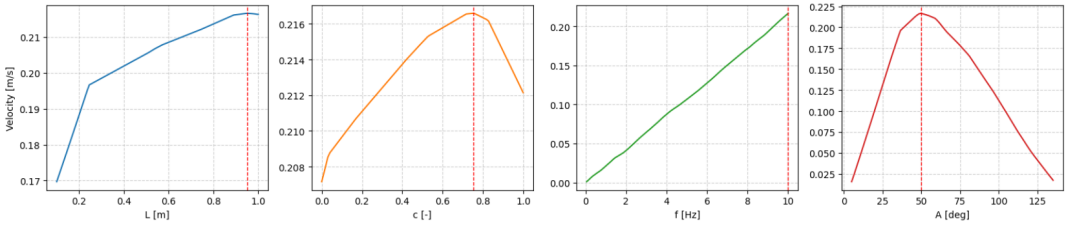

Figure 8: Optimal velocity vs. L, c, f, A

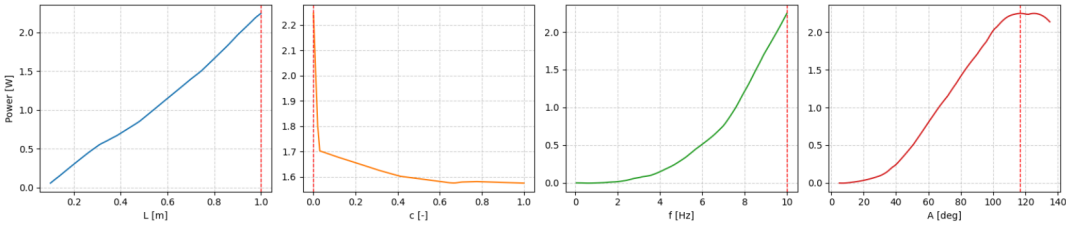

Figure 9: Optimal power vs. L, c, f, A

6 Discussion and conclusion

The proposed data-driven optimization proved effective in identifying passive tentacle configurations that achieve high average thrust and velocity in simulation. The optimal solutions found by the Genetic Algorithm, combined with the surrogate model, span a wide range of performances and are consistent with values reported in the literature for similar systems.

The multi-objective algorithm produced a clear Pareto front, showing that maximizing one metric may penalize the other due to the compliance of the robot, but the method allows for the exploration of optimal compromises. Thrust increases with stiffer compositions and large oscillation amplitudes, while velocity is maximized for slightly more compliant structures and moderate movements. Tentacle length improves performance only up to a certain point, beyond which the increased compliance prevents further gains in speed.

The method could be further improved. Results are currently based solely on computer simulations, without empirical validation. Conducting experimental tests on real prototypes would help bridge the *sim2real* gap, as modeling soft robots is inherently complex and subject to non-idealities. Moreover, the control strategy relies exclusively on a sawtooth signal, truncated at the fourth term of its Fourier series, although alternative waveforms or steeper actuation profiles could be encoded as design variables and may significantly affect performance. Finally, an ideal motor has been considered, but the design criteria did not account for efficiency or energy dissipation parameters, even though these are crucial aspects in the development of feasible underwater robots.

References

[1] Nana Obayashi, Carlo Bosio, and Josie Hughes. “Soft passive swimmer optimization: from simulation to reality using data-driven transformation”. In: *IEEE 5th International Conference on Soft Robotics (RoboSoft)* (2022).